ChemComm

Accepted Manuscript

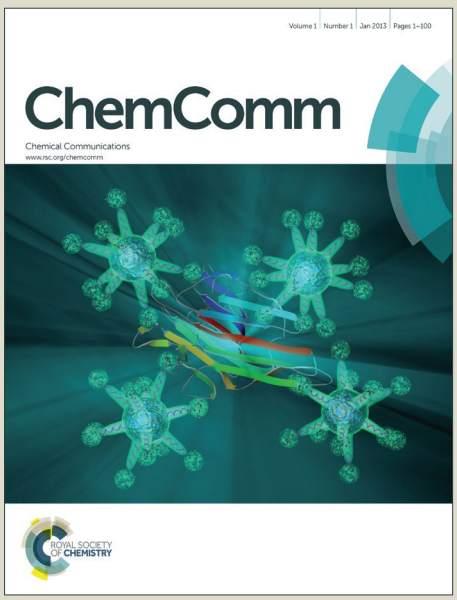

ROYAL SOCIETY OF CHEMISTRY

www.rsc.org/chemcomm

Cite this: DOI: 10.1039/c0xx00000x

www.rsc.org/xxxxxx

ARTICLE TYPE

Leucine zipper pair-based lipid vesicle for image-guided therapy in breast cancer

Eun-Kyung Lim[a], Panki Bae[b], Haeran Kim[b] and Juyeon Jung[*a,c]

Received (in XXX, XXX) Xth XXXXXXXXX 20XX, Accepted Xth XXXXXXXXX 20XX

DOI: 10.1039/b000000x

We developed a controllable image-guided therapy system as a powerful tool for diagnostic and therapeutic applications. The system uses a two-step pretargeting approach that takes advantage of the highly selective binding interactions between leucine zipper pairs. It consists of the utilization of a tumor pretargeting probe for diagnosis and, if necessary, a probe for therapy.

Drugs, toxins, radioisotopes, and other compounds have been conjugated to antibodies and antibody fragments for diagnostic and therapeutic purposes. The explicit specificity of antibodies enables the efficient delivery and accumulation of these compounds at tumor sites.[1-4] Chemotherapy is a major conventional therapeutic approach for the treatment of localized and metastasized cancers; however, the difficulty in reaching therapeutically effective local drug concentrations at the tumor site without damaging surrounding healthy tissue has become a critical obstacle in cancer therapies using chemotherapeutic agents.

An antibody-drug conjugate (ADC) consists of a highly potent drug covalently attached via a linker to an antibody specific to a tumor surface target antigen. Over the past few years, ADCs have emerged as powerful tools in biomedical research, diagnoses, and therapies due to their enhanced specificity and efficacy in the delivery of cytotoxic drugs. Conventional conjugation sites between drugs and antibodies typically include cysteine and lysine residues. The development of ADCs has been challenging because a human IgG comprises a wide distribution of surface-accessible lysine residues and four solvent-exposed disulfide bonds. After conjugation, a number of heterogeneous ADC mixtures with differing drug-to-antibody ratios (DARs) and different conjugation sites is possible and thus, would affect the clinical performance of the ADC.[5-8] A high degree of antibody modification due to overloading a therapeutic or diagnostic agent often results in antibody aggregation, perturbed stability, and decreased ADC half-life in circulation. Recently, theranostic nanomedicine has gained attention as a promising therapeutic paradigm that uses theranostic agents with diagnostic and therapeutic capabilities, low toxicity, enhanced water solubility, good biocompatibility, and ease of surface modification.[9]

Direct targeting systems, in which targeting agents are attached to antitumor drug molecules or vehicles, favor the drug accumulation at tumor lesions.[10] However, pretargeting systems involve the separation of the targeting agents at the tumor lesions from the subsequent delivery of the therapeutic drug molecules, which offer sufficient time for accurate diagnosis and then treat tumor.[10-12] Therefore, these can achieve highly therapeutic effects with low side effects. In this respect, various approaches have been exploited to fabricate the pretargeting systems.[10,11]

Streptavidin-biotin systems have been well-known for pretargeting systems. In these systems, biotinylated antibodies are first localized on the tumor surface, followed by streptavidin, and, finally, radiolabeled, biotinylated effector molecules are introduced to a pre-localized cancer. This system separates the delivery of radionuclides from the slow antibody targeting step.[13, 14] Functional streptavidin exists as a tetramer and irreversibly binds to four molecules of biotin with high affinity ($K_d = 10^{-15}$ M), thereby amplifying the targeting signal. Several studies have demonstrated that the pretargeting approach using the biotin-streptavidin system could improve tumor-to-background ratios with high specificity. However, this approach has several disadvantages, including possible binding interactions between streptavidin on the conjugated antibody and naturally occurring biotin in human plasma, the high immunogenicity of streptavidin, and the nonspecific uptake of streptavidin by the kidney.[15, 16] The leucine zipper motif is approximately 30 amino acid residues long and is known to form a stable dimer of amphiphilic helices. A rigid heterodimer comprising acidic ZE and basic ZR leucine zipper domains has exceptionally high affinity ($K_d = 10^{-15}$ M) and has been used to join chimeric proteins.[17-19] Remarkably, the leucine zipper pair forms stable and precise complexes in aqueous solutions, as evidenced by NMR and crystallography studies.[20,21] Previously, bispecific antibodies have been successfully produced by mediating the dimerization of Fab or scFv fragments via the leucine zipper pair.[22, 23]

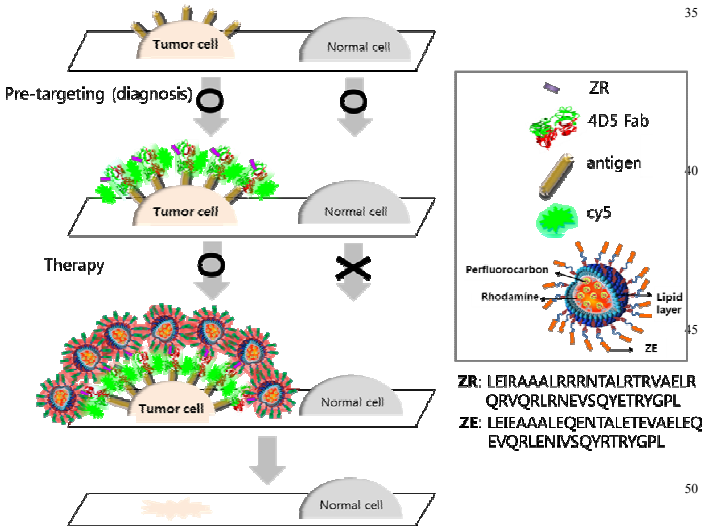

Fig. 1 Schematic representation of the two-step pretargeting approach to cell labeling using leucine zipper pairs. A fluorescently-labeled antibody containing ZR is immobilized on the target antigen overexpressed on the tumor cell surface. Upon localization, the ZE-nanoemulsion is administered and binds to the pretargeted antibody on the tumor cells.

In the present study, we developed a novel image-guided therapy system consisting of a tumor pretargeting probe for diagnosis and, if necessary, a probe for therapy using the highly selective binding interaction between the leucine zipper pair ZR and ZE. The rationale for this approach is illustrated in Fig. 1. Briefly, in the diagnoses and targeting of tumor cells, antibodies fused to leucine zipper domains (ZRs) and labeled with fluorescent dyes target and bind to the targeted antigen with high biological specificity. Subsequently, leucine zipper peptide (ZE)-conjugated nanoemulsions containing therapeutics are administered and attach to the targeted antibody on the tumor cells, enabling image-guided therapy. Importantly, this approach prevents the excessive or unnecessary use of drugs typically practiced in conventional drug delivery systems, wherein targeting and therapy are performed simultaneously regardless of the outcome of diagnostic evaluations. Furthermore, the use of this leucine zipper pair is attractive because there are no known leucine zippers in blood circulation, which provides for highly specific diagnostic and therapeutic outcomes.

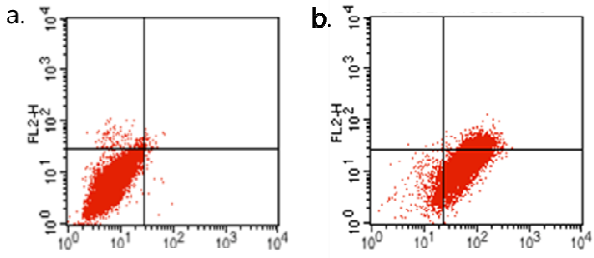

Fig. 2 Flow cytometry analysis of two-step pretargeting of cells. Fluorescein-labeled ZR-4D5 was incubated with MCF10A (a) or SKBR3 (b) cells for 30 min. The pretargeted cells were incubated with ZE-PFC/rhodamine nanoemulsions for 30 min, and the percentage of rhodamine and FITC-labeled cells within the cell population was evaluated.

We employed a Fab fragment derived from the 4D5 monoclonal antibody (IgG1 kappa) against HER2-positive metastatic breast cancer. Intact IgG often requires several days to reach an optimal tumor localization level, leading to severe normal tissue damage. Therefore, antibody fragments without Fc domains are expected to have high target retention and low immunogenicity. A ZR-4D5 Fab (ZR-4D5) fusion gene was synthesized using a secretion signal peptide, 4D5 VH-CH, a $(GGGGS)_3$ flexible linker, ZR, a His tag, a secretion signal peptide, and 4D5 VL-CL, cloned into a pKB-Fab100 vector, and expressed in the *E. coli* strain TG1 via induction with 1 mM isopropyl-1-thio-β-D-galactopyranoside at 30°C overnight. The cells were pelleted and resuspended in periplasmic extraction buffer containing 0.2 M Tris-HCl, 0.5 mM EDTA, and 0.5 mM sucrose at pH 8.0. After centrifugation, soluble 4D5-ZR fragments from the supernatant were purified using protein L agarose beads. The ZR-4D5 was detectable at the predicted size of 50 kDa by SDS-PAGE and western blotting (Fig. S1).

PFC/rhodamine nanoemulsions were prepared by thin film hydration and microfluidization, as previously described.[24-26] Their size distribution and morphology were analyzed using laser scattering (ELS-Z) and transmission electron microscope (TEM) (JEM-2100F), respectively (Fig. S2 in ESI†). ZE peptides were reacted with NHS ligands of the PFC/rhodamine nanoemulsions for 2 h at room temperature. As determined by a fluorescent spectrometer, the emission spectrum of the ZE-PFC/rhodamine nanoemulsion peaked at 600 nm and was similar to that of the PFC/rhodamine nanoemulsion (Fig. S3a). The average size of a ZE-PFC/rhodamine nanoemulsion particle was 123.1±26.9 nm as measured by dynamic light scattering analysis (data not shown). To evaluate the sensitivity and cytotoxicity of the ZE-PFC/rhodamine nanoemulsion, SKBR3 (high HER2/neu expression) and MCF10A (low HER2/neu expression) cells were exposed to various concentrations of the nanoemulsion ranging from 0 to 100 μl/ml over 3 days and evaluated by MTT assays (Fig. S3b). The data showed that these cell lines were viable over a broad range of nanoemulsion concentrations with a CC_{80} above 100 μl/ml, indicating the suitability of these nanoemulsions for biological applications.

The accuracy of the two-step approach of ZR-4D5 pretargeting followed by ZE-PFC/rhodamine nanoemulsion targeting in the SKBR3 cells was evaluated by FACS analysis (Fig. 2). The SKBR3 cells were incubated with fluorescein isothiocyanate (FITC)-labeled ZR-4D5 for 30 min, followed by incubation with the ZE-PFC/rhodamine nanoemulsion. The percentages of FITC and rhodamine-labeled cells within the cell population were determined. The data revealed that approximately 93% of the SKBR3 cells interacted with ZR-4D5-FITC, and 13% of these FITC-positive SKBR3 cells were labeled with rhodamine. This indicated a high and specific immobilization of the ZE-PFC/rhodamine nanoemulsion to the SKBR3 cells via the pre-bound ZR-4D5-FITC. As a negative control, MCF10A cells were first treated with ZR-4D5-FITC and subsequently treated with the ZE-PFC/rhodamine nanoemulsions. Only background levels of FITC or rhodamine-positive cells were observed, demonstrating a low level of nonspecific binding of the

nanoemulsions to the cells.

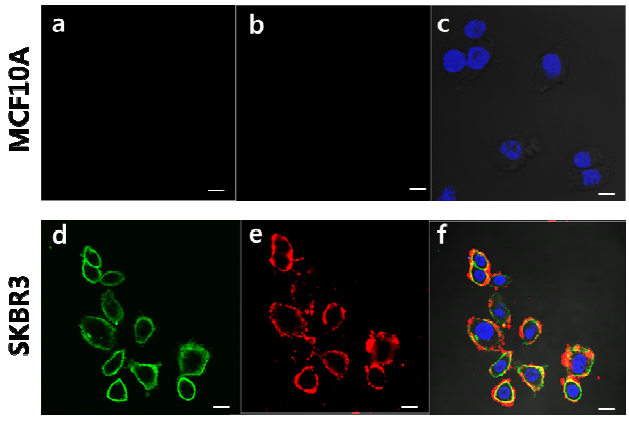

Fig. 3 Fluorescence images of MCF10A and SKBR3 cells after pretreatment with ZR-4D5-FITC (a and d) followed by treatment with ZE-PFC/rhodamine nanoemulsions (b and e). The ZR-4D5-FITC, ZE-PFC/rhodamine nanoemulsion, and DAPI-stained nuclei are shown in green, red, and blue, respectively. Scale bars = 10 μm.

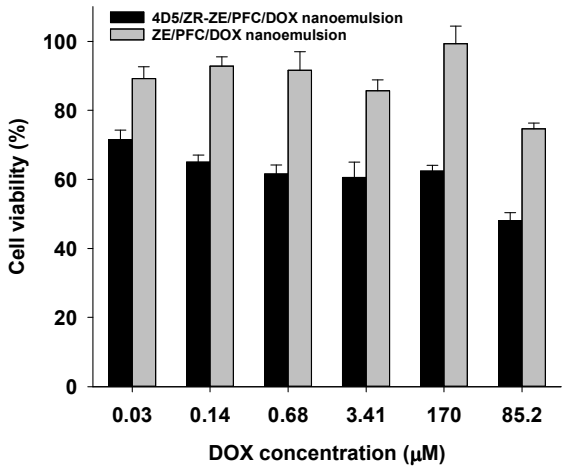

Fig. 4 Cell viability assay results of SKBR3 cells incubated with ZR-4D5 followed by incubation with various concentrations of ZE-PFC/DOX nanoemulsion (4D5/ZR-ZE/PFC/DOX nanomeulsion) or ZE-PFC/DOX nanoemulsion in the absence of ZR-4D5 (ZE/PFC/DOX nanomeulsion).

Fluorescence imaging using Deltavision RT deconvolution microscopy further confirmed the specific binding of ZR-4D5-FITC to the SKBR3 cells and the subsequent binding of the ZE-PFC/rhodamine nanoemulsion (Fig. 3). The successful binding of the ZE-PFC/rhodamine nanoemulsion required the ZR-4D5-FITC pretargeting step to attach to the SKBR3 cell surface. This resulted in an enhanced fluorescent signal. The data indicate that ZR-4D5 specifically binds to the target receptor on the cell surface and that the ZE-PFC/rhodamine nanoemulsion selectively attaches to pretargeted ZR-4D5. As expected, the MCF10A cells did not show any fluorescence signal upon treatment with ZR-4D5-FITC and ZE-PFC/rhodamine nanoemulsion.

The cytotoxicities of ZR-4D5 and the ZE-PFC/doxorubicin (DOX) nanoemulsion complex or of the ZE-PFC/DOX nanoemulsion against SKBR3 and MCF10A cells were evaluated by measuring cell growth inhibition using an MTT assay (Fig. 4).

ZE-PFC/DOX nanoemulsion were prepared in the similar manner as ZE-PFC/rhodamine nanoemulsions (ESI†).[27] DOX loaded in ZE-PFC/DOX nanoelumsions was 0.62 mg/mL by measuring fluorescence (λ_{ex}=490 nm and λ_{em}=590 nm), of which loading efficiency (%) was 62% (loading efficiency (%) = amount of $DOX_{loading}$/amount of DOX_{input}).

We incubated SKBR3 and MCF10A cells (5×10^3 cells/well) in a 96-well plate at 37°C overnight prior to treatment with ZR-4D5 (10 μg/ml). After 30 min, various concentrations of the ZE-PFC/DOX nanoemulsion were incubated with the cells for an additional 30 min. The samples were then washed and kept at 37°C for an additional 72 h. This two-step 4D5-ZR pretargeting followed by ZE-PFC/DOX nanoemulsion targeting showed a remarkably higher treatment efficacy on SKBR3 cells, whereas the other conditions, i.e., ZE-PFC/DOX or PFC/DOX nanoemulsion treatments without 4D5-ZR, did not show any cytotoxicity (Fig. 4 and S4). An *in vitro* DOX release study showed that DOX was gradually released from the ZE-PFC/DOX nanoemulsions over 15 days (Fig. S5).

In conclusion, we developed a controllable two-step pretargeting system using leucine zipper pair to enhance image-guided therapy. The data presented demonstrated that the two-step pretargeting approach was capable of efficiently labeling SKBR3 cells with a pretargeting probe, ZR-4D5, in a diagnosis step, followed by a treatment with an effector probe, ZE-PFC/DOX nanoemulsions, for the subsequent delivery of therapeutics to antibody-targeted sites. The leucine zipper-conjugated pretargeting probes developed in this study provide an alternative means to overcome the limitations of conventional biotin-streptavidin-based targeting systems, such as nonspecific binding to biotin in human plasma and the immunogenicity of biotin and streptavidin. Additionally, this approach provides significant advantages over conventional ADCs and theranostic nanomedicines in which targeting and therapy are often simultaneously performed regardless of the outcome of the diagnostic evaluation. Our approach controls the performance of therapy for limited cases when necessary. We expect that a two-step pretargeting system using leucine zipper pairs will be very useful in many applications, especially to overcome the excessive and unnecessary use of drugs.

The authors acknowledge the financial support from the National Research Foundation of Korea (NRF) Grant funded by the Korea government (NRF-2013M3C1A3064462), BioNano Health-Guard Research Center funded by the Ministry of Science, ICT & Future Planning (MSIP) of Korea as Global Frontier Project (H-GUARD_2014M3A6B2060507) and the KRIBB Initiative Program, Republic of Korea.

[a] *BioNanotechnology Research Center, Korea Research Institute of Bioscience and Biotechnology, 305-806, Daejeon, Republic of Korea, Fax: (+82)-42-879-8594, Tel:(+82)-42-860-4192*

[b] *BioNano Health Guard Research Center, Korea Research Institute of Bioscience and Biotechnology (KRIBB), 305-806, Daejeon, Republic of Korea.*

[c]Nanobiotechnology Major, School of Engineering, University of Science and Technology, 125 Gwahangno, Yuseong, Daejeon 305-806, Republic of Korea.

† Electronic Supplementary Information (ESI) available: Experimental details and supplimentary data. See DOI: 10.1039/b000000x/

Notes and References

1. M. Kuroki, A. Ueno, H. Matsumoto, H. Abe, T. Li, T. Imakiire, Y. Yamauchi, K. Uno, K. Shirota, H. Shibaguchi and M. Kuroki, *Anticancer Res.*, 2002, **22**, 4255-4264.
2. T. Allen, *Nat Rev Cancer.*, 2002, **2**, 750-763.
3. A. Wu and P. Senter, *Nat Biotechnol.*, 2005, **23**, 1137-1146.
4. R. Sharkey and D. Goldenberg, *CA Cancer J Clin.*, 2006, **56**, 226-243.
5. S. AM, Ś. KW and O. J, *Biotechnol Adv.*, 2015, **33**, 775-784.
6. K. Hamblett, P. Senter, D. Chace, M. Sun, J. Lenox, C. Cerveny, K. Kissler, S. Bernhardt, A. Kopcha, R. Zabinski, D. Meyer and J. Francisco, *Clinical cancer research*, 2004, **10**, 7063-7070.
7. L. Wang, G. Amphlett, W. Blättler, J. Lambert and W. Zhang, *Protein Sci.*, 2005, **14**, 2436-2446.
8. D. Willner, P. Trail, S. Hofstead, H. King, S. Lasch, G. Braslawsky, R. Greenfield, T. Kaneko and R. Firestone, *Bioconjug Chem.*, 1993, **4**, 521-527.
9. S. S. Kelkar and T. M. Reineke, *Bioconjugate Chem*, 2011, **22**, 1879-1903.
10. S.-Y. Ain, M.-Y. Peng, L. Rong, H.-Z. Jia, S. Chen, S.-Z. Cheng, J. Feng and X.-Z. Zhang, *Nanoscale*, 2015, **7**, 14786-14793
11. D. M. Goldenberg, J.-F. Charal, J. Barbet, O. Boerman and R. M. Sharkey, *Update Cancer Ther*, 2007, **2**, 19-31
12. R. M. Sharkey, W. J. McBride, H. Karacay, K. Chang, G. L. Griffiths, H.J. Hansenand D.M. Goldenberg, *Cancer res*, 2003, **63**, 354-363
13. K. Hamblett, O. Press, D. Meyer, D. Hamlin, D. Axworthy, D. Wilbur and P. Stayton, *Bioconjug Chem.*, 2005, **16**, 131-138.
14. R. Sharkey, H. Karacay, G. Griffiths, T. Behr, R. Blumenthal, M. Mattes, H. Hansen and D. Goldenberg, *Bioconjug Chem.* , 1997, **8**, 595-604.
15. L. Klumb, V. Chu and P. Stayton, *Biochemistry*, 1998, **37**, 7657-7663.
16. M. Rusckowski, M. Fogarasi, B. Fritz and D. Hnatowich, *Nucl Med Biol.*, 1997, **24**, 263-268.
17. J. Moll, S. Ruvinov, I. Pastan and C. Vinson, *Protein Sci.*, 2001, **10**, 649-655.
18. C. Scott, K. Garcia, F. Carbone, I. Wilson and L. Teyton, *J Exp Med.* , 1996, **183**, 2087-2095.
19. K. Zhang, M. Diehl and D. Tirrell, *J Am Chem Soc.*, 2005, **127**, 10136-10137.
20. Y. Deng, J. Liu, Q. Zheng, Q. Li, N. R. Kallenbach and M. Lu, *Chemistry & Biology*, 2008, **15**, 908-919.
21. S. A. Damesa, R. A. Kammererb, D. Moskauc, J. Engelb and A. T. Alexandrescua, *FEBS letters*, 1999, **446**, 75-80.
22. J. de Kruif and T. Logtenberg, *J Biol Chem.* , 1996, **271**, 7630-7634.
23. S. Kostelny, M. Cole and J. Tso, *J Immunol.* , 1992, **148**, 1547-1553.
24. P. K. Bae, J. Jung, B. H. Chung, *Nano Convergence*, 2014, **1**, 6-16.
25. P. K. Bae and B. H. Chung, *Nano Convergence*, 2014, **1**, 23-31.
26. P. K. Bae and B. H. Chung, *Mol. Imaging Biol.* 2013, **15**, 401-410.
27. P. C. Gokhale, B. Radhakrishnan, S. R. Husain, D. R. Abernethy, R. Sacher, A. Dritschilo, and A. Rahman, *Br. J. Cancer.*, 1996, **74**, 43-48